ACS Macro Letters

pubs.acs.org/macroletters Letter

Theory of Ionic Conductivity with Morphological Control in Polymers

Murugappan Muthukumar*

Cite This: ACS Macro Lett. 2021, 10, 958−964 Read Online

ACCESS | Metrics & More | Article Recommendations

ABSTRACT: We present a general theory of ionic conductivity in polymeric materials consisting of percolated ionic pathways. Identifying two key length scales corresponding to interpath permeation distance ξ and one-dimensional hopping conduction path length $m\lambda$, we have derived closed-form formulas in terms of the energy U required to unbind a conductive ion from its bound state and the partition ratio $\xi/m\lambda$ between the three-dimensional permeation and one-dimensional hopping pathways. The results provide design strategies to significantly enhance ionic conductivity in single-ion conductors. For large barriers to dissociate an ion, corrections to the Arrhenius law are presented. The predicted dependence of ionic conductivity on the unbinding time is in agreement with results in the literature based on simulations and experiments. This theory is generally applicable to conductive systems where the two mechanisms of permeation and hopping occur concurrently.

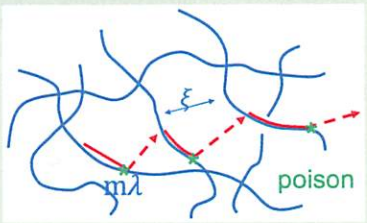

The subject of ionic conductivity in polymeric materials with heterogeneous structures is of intense current interest, primarily due to the societal need for better battery alternatives.[1−33] Significant progress has recently been made toward formulating polymeric materials with enhanced ionic conductivities and at the same time not compromising on their mechanical stability. The procedures that have been implemented in this endeavor are primarily experiments and simulations.[1−33] Generally speaking, the investigated systems include solid polymer electrolytes such as salt-doped poly(ethylene oxide), polymeric single-ion conductors, polymerized ionic liquids, and polyelectrolyte solutions in nanocapillaries.[1−33] The combined approach of precise synthesis of ion-containing polymers, characterization of their assembled structures using a variety of experimental techniques, and molecular modeling has revealed exquisite details on several specific systems and their consequence on the temperature dependence of ionic conductivity. Nevertheless, it is desirable to develop fundamental relations between the heterogeneous structures and the consequent ionic conductivity that are universal instead of treating each system as unique. Such relations would enable design principles to achieve desirable ionic conductivities by tuning the morphology of heterogeneous polymeric materials. With this goal in mind, we present in this Letter a theory for ionic conductivity in polymeric materials with heterogeneous structures.

For illustrative purposes, let us consider three scenarios of general context (Figure 1). The first is pertinent to ion transport in nanoporous media (Figure 1a), where the surface of interconnected pores carry immobile charges and the interior of the pores permit conduction of oppositely charged counterions. In general, the counterions are bound to the charged groups on the interface and the extent of binding depends on the specificity of the ionic species and local dielectric environment. The movement of bound counterions under an external electric field can occur either by hopping (sliding) to its neighboring charged group on the interface or by permeation (conduction) through the interior medium of the pores. These two pathways are indicated by the solid and broken arrows in Figure 1a. In addition to the rigid inorganic porous materials, hydrated Nafion-like organic materials (where interconnected network of hydrophilic domains allow movement of water and cations, but the nonpolar matrix not conducting anions) belong to this general context.

The second scenario is ion conduction in polyelectrolyte solutions. As cartooned in Figure 1b, let us consider semidilute solutions of uniformly charged polyelectrolyte chains where the charge separation along the chain backbone is λ_0 and the correlation length for monomer concentration (mesh size) is ξ. As in the first scenario, ion conduction occurs via the two mechanisms of counterion-hopping along the chain backbone and permeation through the solvent. A typical trajectory of a counterion under an external electric field is a combination of hopping to neighboring sites with spacing λ_0 and permeation through an average mesh size ξ (Figure 1b). Such a situation is also relevant to solutions of polymerized ionic liquids.

Received: April 11, 2021
Accepted: July 2, 2021

https://doi.org/10.1021/acsmacrolett.1c00245
ACS Macro Lett. 2021, 10, 958−964

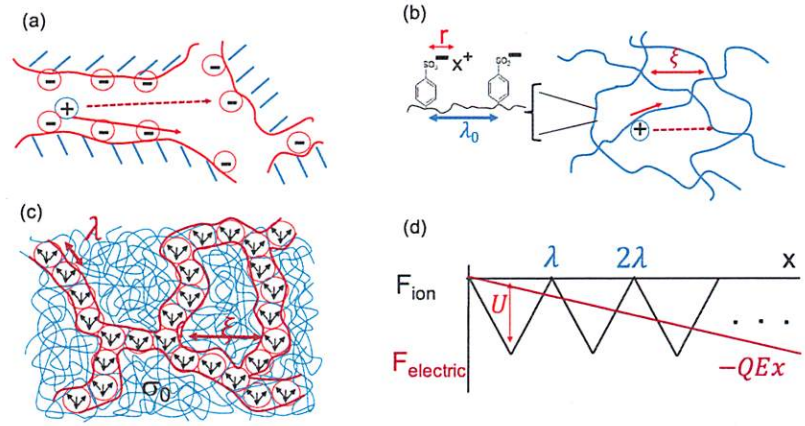

Figure 1. (a) Cartoon of two pathways for ion conduction in nanoporous materials. (b) Sketch of counterion conduction pathways in a semidilute polyelectrolyte solution of mesh size ξ. A chemical example of two adjacent repeat units with charge separation λ_0 is illustrated in the expanded scale. (c) Cartoon of percolating aggregates from ionic clusters constituting the skeletons, where the matrix is permeable to the conducting ion with an intrinsic ionic conductivity σ_0. The average distance between two adjacent ion clusters is λ and the mesh size for the percolating aggregate is ξ. (d) The free energy profile F_{ion} corresponding to sequential unbinding and binding of the conducting ion is periodic, with a free energy barrier U and period λ. The electric energy gain due to externally imposed electric field E is $F_{electric} = -QEx$, where Q is the charge of the ion and x is the location of the ion in the direction of the electric field.

The third scenario is in the context of single-ion conductive ionomers, where many clusters of ion pairs (dipoles) exist as percolated aggregates in a conductive polymer matrix. Examples of the matrix are poly(ethylene oxide) and polycarboxylates and their chemical modifications, and gel polymer electrolytes, which are intrinsically permeable to the conducting ion with ion conductivity σ_0. The percolated aggregates are composed of clusters of ion-pairs formed by multiple chains. Unlike the situation of polyelectrolyte chains, where the ion binding is typically a single ion-pair formation, there are many ion pairs (arising from both intrachain and interchain interactions) in each of the ion clusters. Let the average distance between adjacent ionic clusters along a skeleton of the percolating aggregate be λ and the average mesh size in the background conductive polymer matrix be ξ (Figure 1c). The distance λ between ion clusters constituting a skeleton is related in a complex manner to the spacing of charged groups on the parent polymer chain (analogous to λ_0, but now the spacer moiety is also conductive).

In the context of the above examples, we address ion conduction due to a combination of ion-hopping along a chain or surface (Figures 1a,b) or skeleton of ion clusters (Figure 1c), and permeation through a conductive matrix. There are two length scales that characterize the morphology of the above conducting systems: the average hopping distance λ and the average permeation length ξ. In addition to the these variables characterizing the morphology of the system, the energy U to unbind X^+ (Figure 1b) or its analog in an ion cluster from its corresponding anion is an important variable that controls ionic conductivity due to X^+. In the simplest situation, U for monovalent charges is $U = e^2/(4\pi\epsilon_0\epsilon_{eff}r)$, where e is the electronic charge, ϵ_0 is the permittivity of vacuum, ϵ_{eff} is the effective dielectric constant in the local environment around the bound X^+, and r is the interion distance in an ion pair. In the case of ionic clusters, U arises from collective interactions among all ion pairs inside a cluster and we absorb this important effect through the local effective dielectric constant, which is different from that in the matrix.

Following the law for rates of activated processes, the time τ required to unbind the conducting ion from the ion pair is $\tau = \tau_0 \exp(U/k_BT)$, where τ_0 is the characteristic time for a free conducting ion to diffuse a distance comparable to its linear size, and k_BT is the Boltzmann constant times the absolute temperature. For the purpose of quoting later, the above expressions for U and τ are repeated as

$$U = \frac{e^2}{4\pi\epsilon_0\epsilon_{eff}r}, \quad \tau = \tau_0 \exp\left(\frac{U}{k_BT}\right) \tag{1}$$

In general, the value of τ can be additionally influenced by local segmental dynamics of the polymer as well as collective phonon dynamics of the system.

Consider a one-dimensional ionic conductor where the binding sites for the drifting ion are uniformly present with a period λ. When the applied electric field is not too strong, the moving ion undergoes a series of binding and unbinding at every binding site. This process continues periodically until the ion reaches its favored electrode. Let us denote the free energy profile associated with unbinding of an ion at one location and binding back at the next neighboring binding site at a distance λ as a symmetric triangular free energy barrier of height U (Figure 1d). Therefore, the free energy landscape $F_{ion}(x)$ due to binding and unbinding along the direction x of the constant electric field E is as depicted in Figure 1d with a period λ. The electric contribution to the free energy profile of the ion is $F_{electric}(x) = -QEx$, where $Q = z_+e$ (z_+ is the valency of the conducting ion). The net free energy profile is

$$F(x) = F_{ion}(x) + F_{electric}(x) \tag{2}$$

In addition to the one-dimensional hopping pathway for ion conduction (Figure 1d), we allow a second pathway of ion permeation from one linear assembly of binding sites to another linear assembly of binding sites as cartooned in Figure 2a. In the case of polyelectrolyte solutions, these two pathways can also be labeled as "intrachain" and "interchain" conduction pathways, respectively; for ionic aggregates, these are, respectively, intraskeleton and interskeleton pathways. Assessment of the

https://doi.org/10.1021/acsmacrolett.1c00245
ACS Macro Lett. 2021, 10, 958−964

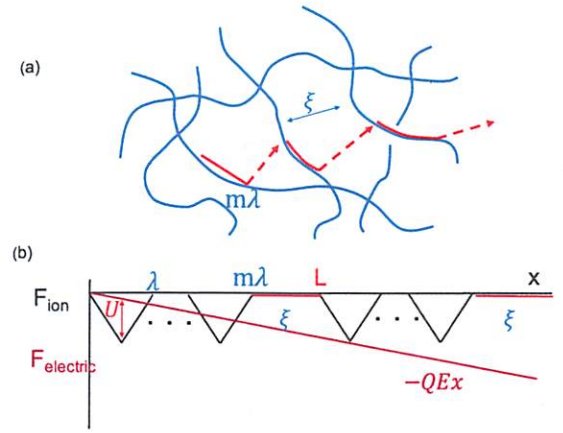

Figure 2. (a) Sketch of the permeation mechanism over a distance ξ through the matrix that occurs in parallel to one-dimensional hopping conduction over a distance $m\lambda$. (b) The corresponding free energy landscape, where L is the period, λ is the subperiod, U is the barrier height, and ξ is the permeation distance.

relative contributions from the intra- and interconduction pathways is of considerable interest in the general contexts mentioned in Figure 1.

In view of the above considerations, we present an analytically tractable theory for the model sketched in Figure 2a, where the curved lines represent hopping pathways and empty space represent permeation pathways. Let there be an infinite number of periods of length L, where each period is labeled by the index $N \geq 1$. In each period, there are m subperiods for one-dimensional conduction, followed by a three-dimensional hopping over a distance ξ through the matrix. Let the regular subperiod for one-dimensional unbinding−binding process be λ. Since ion hopping occurs along the curvilinear contour, we take λ as the average distance between adjacent binding sites projected on the direction of the external electric field. Let n denote the label of the subperiod, $1 \leq n \leq m$. In each subperiod, we take the free energy profile as triangular with barrier height U, as shown in Figure 2a. The periodic free energy profile in the absence of the external electric field is given as

$$F_{\text{ion}}(NL + x) = F_{\text{ion}}(x), \quad N \geq 1 \tag{3}$$

and for each $N \geq 1$,

$$F_{\text{ion}}(n\lambda + x) = F_{\text{ion}}(x), \quad 1 \leq n < m, \quad 0 < x < \lambda \tag{4}$$

In addition to the periodic profile, the applied electric field gives the down hill free energy contribution $-QEx$. Adding $F_{\text{ion}}(x)$ and $F_{\text{electric}}(x)$, the free energy profile for the first period follows as

$$F(x) = \begin{cases} -\frac{2U}{\lambda}[x - (n-1)\lambda] - QEx, & (n-1)\lambda \leq x \leq \left(n - \frac{1}{2}\right)\lambda \\ -2U + \frac{2U}{\lambda}[x - (n-1)\lambda] - QEx, & \left(n - \frac{1}{2}\right)\lambda \leq x \leq n\lambda \\ -QExm\lambda \leq x \leq L = m\lambda + \xi \end{cases} \tag{5}$$

The same result is applicable to other periods as well, with x in the electric field contribution taken as the distance from the origin.

The Langevin equation for the dynamics of the ion at position x and time t is given as

$$\zeta\frac{dx}{dt} = -\frac{\partial F(x)}{\partial x} + \sqrt{\zeta k_B T}\Gamma(t) \tag{6}$$

where ζ is the friction coefficient of the ion in the matrix and $\Gamma(t)$ is the random noise taken to be white noise satisfying the fluctuation−dissipation theorem,

$$\langle\Gamma(t)\rangle = 0, \ \langle\Gamma(t)\Gamma(t')\rangle = 2\delta(t - t') \tag{7}$$

where the angular brackets denote the averaging over the probability distribution function $P(x, t)$ of finding the ion at position x and time t. Identifying the diffusion coefficient D of the ion in the matrix as $D = k_B T/\zeta$, eq 6 becomes

$$\frac{dx}{dt} = -D\frac{\partial F(x)/k_B T}{\partial x} + \sqrt{D}\Gamma(t) \tag{8}$$

Performing the average over $P(x, t)$, the above equation gives the average velocity v as

$$v = \left\langle \frac{dx}{dt} \right\rangle = -D\left\langle \frac{\partial}{\partial x}(F(x)/k_B T) \right\rangle \tag{9}$$

where $\langle\Gamma(t)\rangle = 0$ from eq 7 is used. Note that, if there are no barriers and there is only electrophoretic drift, $F(x) = -QEx$, then $v = \frac{QD}{k_B T}E$ so that the ionic conductivity $\sigma_0 = Qv/E$ is given by $Q^2D/k_B T$. In the presence of barriers, the ionic conductivity σ is modified from this result and can generally be represented in terms of an effective diffusion coefficient $D_{\text{eff}}(U, E)$ which depends on the barrier height U and E,

$$\sigma_0 = \frac{Q^2 D}{k_B T}, \quad \sigma = \frac{\sigma_0}{D_0}D_{\text{eff}}(U, E) \tag{10}$$

Note that D corresponds to ion diffusion in the matrix and it depends on the various ion hopping processes involving the barriers in the matrix, that are responsible for ion conduction in the matrix.

The derivation of σ is as follows. We calculate the average velocity v of the ion from eq 9 using $P(x, t)$ and get σ from the relation $\sigma = Qv/E$. The probability distribution function $P(x, t)$ follows from the Fokker−Planck formalism of the Langevin equation (eq 8) as[34,35]

$$\frac{\partial P(x, t)}{\partial t} = -\frac{\partial}{\partial x}J(x, t) \tag{11}$$

$$J(x, t) = -D\left[\left(\frac{\partial F(x)/k_B T}{\partial x}\right)P(x, t) + \frac{\partial P(x, t)}{\partial x}\right] \tag{12}$$

In the steady state where the flux J is constant, integration of eq 12 from $x = 0$ gives

$$P(x) = e^{-F(x)/k_B T}\left[P(x = 0) - \frac{J}{D}\int_0^x dx' e^{F(x')/k_B T}\right] \tag{13}$$

$P(x = 0)$ is determined from $P(NL + x)$ given by the above equation. Using eq 5, the integral on the right-hand side of eq 13 becomes

$$\int_0^{NL+x} dx' e^{F(x')/k_B T} = I_+\frac{(1 - e^{-NQEL/k_B T})}{(1 - e^{-QEL/k_B T})} + e^{-NQEL/k_B T}\int_0^x dx' e^{F(x')/k_B T} \tag{14}$$

where

https://doi.org/10.1021/acsmacrolett.1c00245
ACS Macro Lett. 2021, 10, 958−964

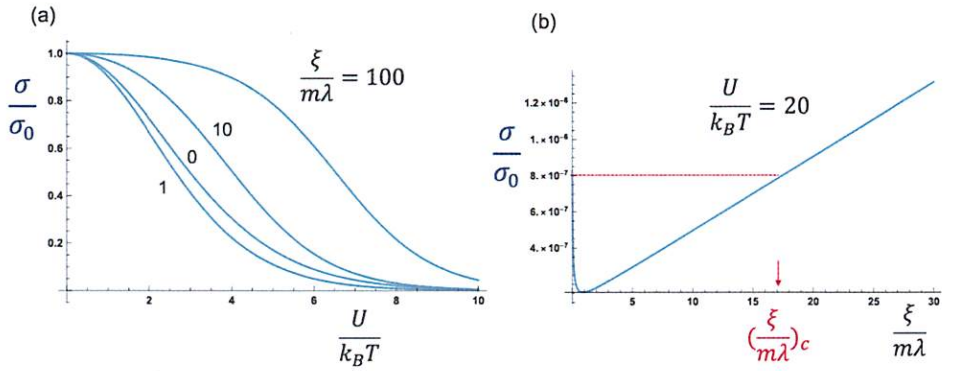

Figure 3. (a) Plot of σ/σ_0 given by eq 28 vs U/k_BT for different values of the partition ratio $\xi/m\lambda$. (b) Nonmonotonic dependence of σ/σ_0 on the partition ratio for $U = 20k_BT$. Beyond the critical value $(\xi/m\lambda)_c$, ionic conductivity is enhanced compared to the case of no permeation pathway.

$$I_+ = \int_0^L \mathrm{d}x e^{F(x)/k_BT} \tag{15}$$

Combining eqs 13 and 14, we get

$$P(NL + x) = e^{NQEL/k_BT - F(x)/k_BT}\left[P(x = 0) - \frac{J}{D}\frac{I_+}{(1 - e^{-QEL/k_BT})}\right] + e^{-F(x)/k_BT}\left[\frac{J}{D}\frac{I_+}{(1 - e^{-QEL/k_BT})} - \frac{J}{D}\int_0^x \mathrm{d}x' e^{F(x')/k_BT}\right] \tag{16}$$

Since $P(NL + x)$ must be finite for $N \to \infty$,

$$P(x = 0) = \frac{J}{D}\frac{I_+}{(1 - e^{-QEL/k_BT})} \tag{17}$$

and, hence, we get from eqs 13 and 16

$$P(NL + x) = P(x) \tag{18}$$

Because of periodicity, $P(x)$ is normalized in every period so that

$$\int_0^L \mathrm{d}x P(x) = L \tag{19}$$

Substituting eq 17 into eq 13 and performing the integration from $x = 0$ to $x = L$, we get

$$J = DL\frac{(1 - e^{-QEL/k_BT})}{[I_+I_- - (1 - e^{-QEL/k_BT})Y]} \tag{20}$$

where

$$I_- = \int_0^L \mathrm{d}x e^{-F(x)/k_BT} \tag{21}$$

and

$$Y = \int_0^L \mathrm{d}x e^{-F(x)/k_BT}\int_0^x \mathrm{d}x' e^{F(x')/k_BT} \tag{22}$$

The velocity of the ion follows from eqs 9 and 12 as

$$v = \frac{1}{L}\int_0^L \mathrm{d}x\left[J + D\frac{\partial P(x)}{\partial x}\right] = J \tag{23}$$

where the periodicity property $P(L) = P(0)$ is used. The general expression for the ionic conductivity, $\sigma = Qv/E$, is given by eqs 20 and 23 as

$$\sigma = \frac{QDL}{E}\frac{(1 - e^{-QEL/k_BT})}{[I_+I_- - (1 - e^{-QEL/k_BT})Y]} \tag{24}$$

where I_+, I_-, and Y are given in eqs 15, 21, and 22, respectively.

Focusing on the linear response regime (Ohm's regime), namely, $QE\lambda < k_BT$, the ionic conductivity is given by

$$\sigma = \frac{Q^2DL^2}{k_BT}\frac{1}{I_+(\vec{E}0)I_-(\vec{E}0)} \tag{25}$$

where $I_+(E \to 0)$ and $I_-(E \to 0)$ follow from eqs 15 and 21 as

$$I_+(\vec{E}0) = -m\lambda\left(\frac{k_BT}{U}\right)(e^{-U/k_BT} - 1) + \xi \tag{26}$$

$$I_-(\vec{E}0) = -m\lambda\left(\frac{k_BT}{U}\right)(1 - e^{U/k_BT}) + \xi \tag{27}$$

The substitution of eqs 26 and 27 into eq 25 yields a general expression for ionic conductivity in the linear regime as

$$\frac{\sigma}{\sigma_0} = \left(1 + \frac{\xi}{m\lambda}\right)^2\frac{(U/k_BT)^2}{\left[e^{U/k_BT} - 1 + \frac{U}{k_BT}\left(\frac{\xi}{m\lambda}\right)\right]\left[1 - e^{-U/k_BT} + \frac{U}{k_BT}\left(\frac{\xi}{m\lambda}\right)\right]} \tag{28}$$

Note that the right-hand side can be interpreted as D_{eff} in units of D, as defined in eq 10. As is evident from eq 28, the ratio σ/σ_0 of ionic conductivity at T to that at $T \to \infty$ depends on two key parameters, namely, U/k_BT and $\xi/m\lambda$. As already noted, U/k_BT is dictated by the specificity of the ion pairs. The second factor $\xi/m\lambda$ is the partition ratio of the permeation length ξ through the matrix to the hopping distance along a one-dimensional trajectory. This partition ratio is a measure of structural heterogeneity in the material. For large barriers $U/k_BT \gg 1$, eq 28 reduces to the limiting laws

$$\frac{\sigma}{\sigma_0} = \begin{cases} \left(\frac{U}{k_BT}\right)^2 e^{-U/k_BT}\frac{\xi}{m\lambda} = 0, & \frac{U}{k_BT} \gg 1 \\ \left(\frac{\xi}{m\lambda}\right)\left(\frac{U}{k_BT}\right)e^{-U/k_BT}\frac{\xi}{m\lambda} \gg 1, & \frac{U}{k_BT} \gg 1 \end{cases} \tag{29}$$

Evidently, the temperature dependence of ionic conductivity is not simply the Arrhenius behavior due to the presence of the prefactors that depend on the barrier height.

The dependence of σ/σ_0 on U and the partition ratio $\xi/m\lambda$ given by eq 28 is presented in Figure 3a. The extent of decrease

https://doi.org/10.1021/acsmacrolett.1c00245
ACS Macro Lett. 2021, 10, 958−964

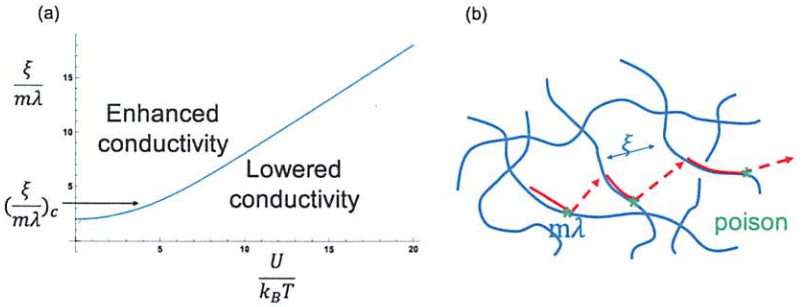

Figure 4. (a) Plot of the threshold value $(\xi/m\lambda)_c$ vs U/k_BT. For partition ratios larger than the threshold value ionic conductivity is enhanced, and for partition ratios below the threshold value, conductivity is lowered. (b) Enhancement of ionic conductivity by designing chemical routes to interrupt one-dimensional conduction at $m\lambda$ by creating a poison and to force the ion into permeation mechanism.

in σ/σ_0 with an increase in U/k_BT depends on the partition ratio. As seen in Figure 3a, σ/σ_0 first decreases with $\xi/m\lambda$ and then increases for higher values of $\xi/m\lambda$. This nonmonotonic behavior is illustrated in Figure 3b for $U = 20k_BT$. The initial decrease is due to the inefficiency of the permeation pathway for such short ξ, namely, the loosened ion from its binding site immediately returns back to the same binding site. For larger permeation distances, the ion escapes from the binding traps along its original path. The minimum value of σ/σ_0 occurs at $(\xi/m\lambda)^*$ given by

$$\left(\frac{\xi}{m\lambda}\right)^* = \frac{(a+b)(U/k_BT) - 2ab}{(a+b)(U/k_BT) - 2(U/k_BT)^2} \tag{30}$$

where a and b are defined as

$$a = (1 - e^{-U/k_BT}), \quad b = (e^{U/k_BT} - 1) \tag{31}$$

For large barriers as illustrated in Figure 3b, $\left(\frac{\xi}{m\lambda}\right)^* \to 1$.

As the partition ratio is increased from $\left(\frac{\xi}{m\lambda}\right)^*$, there exists a threshold value $\left(\frac{\xi}{m\lambda}\right)_c$ beyond which the conductivity is above the value when the permeation mechanism is absent. This is shown in Figure 3b for $U = 20k_BT$. In general, the dependence of $\left(\frac{\xi}{m\lambda}\right)_c$ on U/k_BT is given by

$$\left(\frac{\xi}{m\lambda}\right)_c = \frac{2ab - (a+b)U/k_BT}{(U/k_BT)^2 - ab} \tag{32}$$

where a and b are given in eq 31. This result is plotted in Figure 4a, which delineates the regime of enhanced conductivity ($\xi/m\lambda > (\xi/m\lambda)_c$) and lowered conductivity ($\xi/m\lambda < (\xi/m\lambda)_c$) due to access to the permeation mechanism. For large barriers, $(\xi/m\lambda)_c \simeq U/k_BT$, consistent with the crossover behavior between the two limits given in eq 29.

The prediction from eq 28 and Figure 4a provides a design strategy to significantly enhance ionic conductivity in heterogeneous structures. For example, if the one-dimensional conductive pathway is blocked at $m\lambda$ by doping the polymer chain with a nonconductive segment which functions as a poison (Figure 4b), then the permeation mechanism is forced on the conducting ion resulting in enhanced conduction for $\xi/m\lambda > (\xi/m\lambda)_c$.

In summary, a general theory for ionic conductivity in heterogeneous polymer structures is derived in terms of the energy U to unbind a conductive ion from the polymer backbone and the partition ratio $\xi/m\lambda$ between three-dimensional permeation and one-dimensional conduction. For large barriers, the conductivity is pseudo-Arrhenius, with the prefactor of the exponential Arrhenius term depending on U and $\xi/m\lambda$, as given in eq 29. The prefactor can significantly affect the deduction of the activation barrier based on the standard practice of using the Arrhenius form. For example, according to the Arrhenius form, the temperature dependence of $\log_{10}(\sigma/\sigma_0)$ versus $1/T$ is given by the bottom line in Figure 5 for $U = 100$ kJ/mol and $\xi/m\lambda = 0$. On the other hand, the use of eq 28 gives the intermediate curve for the same values of U and $\xi/m\lambda$ as for the bottom line. The conductivity is higher by more than an order of magnitude. If $\xi/m\lambda > (\xi/m\lambda)_c$, then the conductivity is even higher, as illustrated by the top curve for $\xi/m\lambda = 100$. If the middle curve were to be fitted with the Arrhenius form, the inferred U is approximately 75 kJ/mol. Therefore, the true free energy barrier is actually higher than the value obtained from direct implementation of the Arrhenius form.

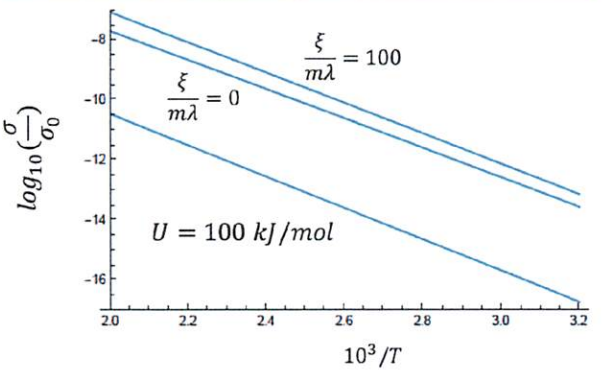

Figure 5. Plot of σ/σ_0 vs $1/T$ for $U = 100$ kJ/mol. Bottom line: Arrhenius plot; middle and top curves are from eq 28 with $\xi/m\lambda = 0$ and 100, respectively.

The limits given in eq 29 can be equivalently represented in terms of the unbinding time τ (eq 1) as

$$\frac{\sigma}{\sigma_0} = \left(\frac{\tau}{\tau_0}\right)^{-1} \ln^y\left(\frac{\tau}{\tau_0}\right) \tag{33}$$

where $y = 1$ and 2 for $\xi/m\lambda \gg 1$ and $\xi/m\lambda = 0$, respectively. The value of the exponent y can be slightly different if the free energy profile in every subperiod is smoother than the triangular profile used here. Ignoring the weak logarithmic corrections, we get

$$\sigma \sim \tau^{-1} \tag{34}$$

https://doi.org/10.1021/acsmacrolett.1c00245
ACS Macro Lett. 2021, 10, 958−964

This general prediction valid for large barriers is consistent with prior simulation and experimental results in the literature.[12,27,31] If the barrier is weak, the full expression given in eq 28 needs to be used in conjunction with eq 1 to obtain the τ-dependence of the ionic conductivity.

Although the theory is presently couched in the context of single-ion conductors in dense heterogeneous polymer systems, it is applicable to polyelectrolyte solutions and polymerized ionic liquids as well where interchain hopping mechanism is prevalent in addition to intrachain ion conduction. The present general theory addressing simultaneous occurrence of hopping and permeation pathways is applicable to systems such as nanoporous materials, polyelectrolyte solutions, hydrated ionomers, polymerized ionic liquids, and ion-containing polymers with ion-containing matrices (either due to added solvent or highly polar polymer backbone like poly(ethylene oxide)). Obviously, the permeation pathway is absent if the matrix is not conductive; now, σ_0 denotes the conductivity in the infinite temperature limit. Additional features to the present model such as local segmental dynamics and collective phonon modes can be of importance. Assessment of contributions from these effects to ionic conductivity is relegated to future work.

AUTHOR INFORMATION

Corresponding Author

Murugappan Muthukumar − *Department of Polymer Science and Engineering, University of Massachusetts, Amherst, Massachusetts 01003, United States;* orcid.org/0000-0001-7872-4883; Email: muthu@polysci.umass.edu

Complete contact information is available at: https://pubs.acs.org/10.1021/acsmacrolett.1c00245

Notes

The author declares no competing financial interest.

ACKNOWLEDGMENTS

The author is grateful to his colleague Bryan Coughlin for stimulating discussions. Acknowledgement is made to the National Institutes of Health (Grant No. 5R01HG002776-16), National Science Foundation (Grant No. DMR 2004493), and AFOSR (Grant No. FA9550-20-1-0142).

REFERENCES

(1) Bordi, F.; Cametti, C.; Colby, R. H. Dielectric spectroscopy and conductivity of polyelectrolyte solutions. *J. Phys.: Condens. Matter* **2004**, *16*, R1423−R1463.

(2) Beers, K. M.; Balsara, N. P. Design of Cluster-free Polymer Electrolyte Membranes and Implications on Proton Conductivity. *ACS Macro Lett.* **2012**, *1*, 1155−1160.

(3) Hall, L. M.; Stevens, M. J.; Frischknecht, A. L. Dynamics of Model Ionomer Melts of Various Architectures. *Macromolecules* **2012**, *45*, 8097−8108.

(4) Choi, J.-H.; Ye, Y.; Elabd, Y. A.; Winey, K. I. Network Structure and Strong Microphase Separation for High Ion Conductivity in Polymerized Ionic Liquid Block Copolymers. *Macromolecules* **2013**, *46*, 5290−5300.

(5) Buitrago, C. F.; Jenkins, J. E.; Opper, K. L.; Aitken, B. S.; Wagener, K. B.; Alam, T. M.; Winey, K. I. Room Temperature Morphologies of Precise Acid-and Ion-Containing Polyethylenes. *Macromolecules* **2013**, *46*, 9003−9012.

(6) Bolintineanu, D. S.; Stevens, M. J.; Frischknecht, A. L. Influence of Cation Type on Ionic Aggregates in Precise Ionomers. *Macromolecules* **2013**, *46*, 5381−5392.

(7) Bolintineanu, D. S.; Stevens, M. J.; Frischknecht, A. L. Atomistic Simulations Predict a Surprising Variety of Morphologies in Precise Ionomers. *ACS Macro Lett.* **2013**, *2*, 206−210.

(8) Mohd Noor, S. A.; Gunzelmann, D.; Sun, J.; MacFarlane, D. R.; Forsyth, M. Ion Conduction and Phase Morphology in Sulfonate Copolymer Ionomers Based on Ionic Liquid-Sodium Cation Mixtures. *J. Mater. Chem. A* **2014**, *2*, 365−374.

(9) Noor, S. A. M.; Sun, J.; Macfarlane, D. R.; Armand, M.; Gunzelmann, D.; Forsyth, M. Decoupled Ion Conduction in Poly(2-Acrylamido-2-Methyl-1-Propane-Sulfonic Acid) Homopolymers. *J. Mater. Chem. A* **2014**, *2*, 17934−17943.

(10) Singh, S. P.; Muthukumar, M. Electrophoretic Mobilities of Counterions and a Polymer in Cylindrical Pores. *J. Chem. Phys.* **2014**, *141*, 114901.

(11) Fan, F.; Wang, Y.; Hong, T.; Heres, M. F.; Saito, T.; Sokolov, A. P. Ion Conduction in Polymerized Ionic Liquids with Different Pendant Groups. *Macromolecules* **2015**, *48*, 4461−4470.

(12) Mogurampelly, S.; Keith, J. R.; Ganesan, V. Mechanisms Underlying Ion Transport in Polymerized Ionic Liquids. *J. Am. Chem. Soc.* **2017**, *139*, 9511−9514.

(13) Iacob, C.; Matsumoto, A.; Brennan, M.; Liu, H.; Paddison, S. J.; Urakawa, O.; Inoue, T.; Sangoro, J.; Runt, J. Polymerized Ionic Liquids: Correlation of Ionic Conductivity with Nanoscale Morphology and Counterion Volume. *ACS Macro Lett.* **2017**, *6*, 941−946.

(14) Delhorbe, V.; Bresser, D.; Mendil-Jakani, H.; Rannou, P.; Bernard, L.; Gutel, T.; Lyonnard, S.; Picard, L. Unveiling the Ion Conduction Mechanism in Imidazolium-Based Poly(Ionic Liquids): A Comprehensive Investigation of the Structure-to-Transport Interplay. *Macromolecules* **2017**, *50*, 4309−4321.

(15) Kusoglu, A.; Weber, A. Z. New Insight into Perfluorinated Sulfonic-Acid Ionomers. *Chem. Rev.* **2017**, *117*, 987−1104.

(16) Wang, S.-W.; Colby, R. H. Linear Viscoelasticity and Cation Conduction in Polyurethane Sulfonate Ionomers with Ions in the Soft Segment-Single Phase Systems. *Macromolecules* **2018**, *51*, 2757−2766.

(17) Stacy, E. W.; Gainaru, C. P.; Gobet, M.; Wojnarowska, Z.; Bocharova, V.; Greenbaum, S. G.; Sokolov, A. P. Fundamental Limitations of Ionic Conductivity in Polymerized Ionic Liquids. *Macromolecules* **2018**, *51*, 8637−8645.

(18) Cheng, Y.; Yang, J.; Hung, J.-H.; Patra, T. K.; Simmons, D. S. Design Rules for Highly Conductive Polymeric Ionic Liquids from Molecular Dynamics Simulations. *Macromolecules* **2018**, *51*, 6630−6644.

(19) Enokida, J. S.; Tanna, V. A.; Winter, H. H.; Coughlin, E. B. Progression of the Morphology in Random Ionomers Containing Bulky Ammonium Counterions. *Macromolecules* **2018**, *51*, 7377−7385.

(20) Rank, C.; Yan, L.; Mecking, S.; Winey, K. I. Periodic Polyethylene Sulfonates from Polyesterification: Bulk and Nanoparticle Morphologies and Ionic Conductivities. *Macromolecules* **2019**, *52*, 8466−8475.

(21) Frischknecht, A. L.; Winey, K. I. The Evolution of Acidic and Ionic Aggregates in Ionomers during Microsecond Simulations. *J. Chem. Phys.* **2019**, *150*, 064901.

(22) Frischknecht, A. L.; Paren, B. A.; Middleton, L. R.; Koski, J. P.; Tarver, J. D.; Tyagi, M.; Soles, C. L.; Winey, K. I. Chain and Ion Dynamics in Precise Polyethylene Ionomers. *Macromolecules* **2019**, *52*, 7939−7950.

(23) Paren, B. A.; Thurston, B. A.; Neary, W. J.; Kendrick, A.; Kennemur, J. G.; Stevens, M. J.; Frischknecht, A. L.; Winey, K. I. Percolated Ionic Aggregate Morphologies and Decoupled Ion Transport in Precise Sulfonated Polymers Synthesized by Ring-Opening Metathesis Polymerization. *Macromolecules* **2020**, *53*, 8960−8973.

(24) Bostwick, J. E.; Zanelotti, C. J.; Iacob, C.; Korovich, A. G.; Madsen, L. A.; Colby, R. H. Ion Transport and Mechanical Properties of Non-Crystallizable Molecular Ionic Composite Electrolytes. *Macromolecules* **2020**, *53*, 1405−1414.

(25) Schauser, N. S.; Grzetic, D. J.; Tabassum, T.; Kliegle, G. A.; Le, M. L.; Susca, E. M.; Antoine, S.; Keller, T. J.; Delaney, K. T.; Han, S.; Seshadri, R.; Fredrickson, G. H.; Segalman, R. A. The Role of Backbone Polarity on Aggregation and Conduction of Ions in Polymer Electrolytes. *J. Am. Chem. Soc.* **2020**, *142*, 7055−7065.

(26) Bocharova, V.; Sokolov, A. P. Perspectives for Polymer Electrolytes: A View from Fundamentals of Ionic Conductivity. *Macromolecules* **2020**, *53*, 4141−4157.
(27) Jones, S. D.; Schauser, N. S.; Fredrickson, G. H.; Segalman, R. A. The Role of Polymer-Ion Interaction Strength on the Viscoelasticity and Conductivity of Solvent-Free Polymer Electrolytes. *Macromolecules* **2020**, *53*, 10574−10581.
(28) Liu, J.; Pickett, P. D.; Park, B.; Upadhyay, S. P.; Orski, S. V.; Schaefer, J. L. Non-Solvating, Side-Chain Polymer Electrolytes as Lithium Single-Ion Conductors: Synthesis and Ion Transport Characterization. *Polym. Chem.* **2020**, *11*, 461−471.
(29) Yan, L.; Hoang, L.; Winey, K. I. Ionomers from Step-Growth Polymerization: Highly Ordered Ionic Aggregates and Ion Conduction. *Macromolecules* **2020**, *53*, 1777−1784.
(30) Yan, L.; Rank, C.; Mecking, S.; Winey, K. I. Gyroid and Other Ordered Morphologies in Single-Ion Conducting Polymers and Their Impact on Ion Conductivity. *J. Am. Chem. Soc.* **2020**, *142*, 857−866.
(31) Bollinger, J. A.; Stevens, M. J.; Frischknecht, A. L. Quantifying Single-Ion Transport in Percolated Ionic Aggregates of Polymer Melts. *ACS Macro Lett.* **2020**, *9*, 583−587.
(32) Zhang, Z.; Wheatle, B. K.; Krajniak, J.; Keith, J. R.; Ganesan, V. Ion Mobilities, Transference Numbers, and Inverse Haven Ratios of Polymeric Ionic Liquids. *ACS Macro Lett.* **2020**, *9*, 84−89.
(33) Schauser, N. S.; Nikolaev, A.; Richardson, P. M.; Xie, S.; Johnson, K.; Susca, E. M.; Wang, H.; Seshadri, R.; Clement, R. J.; de Alaniz, J. R.; Segalman, R. A. Glass Transition Temperature and Ion Binding Determine Conductivity and Lithium-Ion Transport in Polymer Electrolytes. *ACS Macro Lett.* **2021**, *10*, 104−109.
(34) Muthukumar, M. Charge, Diffusion, and Mobility of Proteins Through Nanopores. *J. Chem. Phys.* **2014**, *141*, 081104.
(35) Risken, H. *The Fokker-Planck Equation*; Springer: Berlin, Germany, 1989.

https://doi.org/10.1021/acsmacrolett.1c00245
ACS Macro Lett. 2021, 10, 958−964